Journal of Applied and Computational Mechanics

Nonlinear Dynamic Response of Functionally Graded Porous Plates on Elastic Foundation Subjected to Thermal and Mechanical Loads

Nguyen Dinh Duc[1,2], Vu Dinh Quang[1,2], Pham Dinh Nguyen[1], Trinh Minh Chien[3]

[1] Advanced Materials and Structures Laboratory, VNU-Hanoi - University of Engineering and Technology (UET),
Hanoi, 100000, Vietnam, ducnd@vnu.edu.vn

[2] Infrastructure Engineering Program -VNU-Hanoi, Vietnam-Japan University (VJU),
Hanoi, 100000, Vietnam

[3] Department of Civil and Environmental Engineering, Sejong University, 98 Gunja Dong, Gwangjin Gu, Seoul, 143-747, South Korea

Abstract. In this paper, the first-order shear deformation theory is used to derive theoretical formulations illustrating the nonlinear dynamic response of functionally graded porous plates under thermal and mechanical loadings supported by Pasternak's model of the elastic foundation. Two types of porosity including evenly distributed porosities (Porosity-I) and unevenly distributed porosities (Porosity-II) are assumed as effective properties of FGM plates such as Young's modulus, the coefficient of thermal expansion, and density. The strain-displacement formulations using Von Karman geometrical nonlinearity and general Hooke's law are used to obtain constitutive relations. Airy stress functions with full motion equations which is employed to shorten the number of governing equations along with the boundary and initial conditions lead to a system of differential equations of the nonlinear dynamic response of porous FGM plates. Considering linear parts of these equations, natural frequencies of porous FGM plates are determined. By employing Runge-Kutta method, the numerical results illustrate the influence of geometrical configurations, volume faction index, porosity, elastic foundations, and mechanical as well as thermal loads on the nonlinear dynamic response of the plates. Good agreements are obtained in comparison with other results in the literature.

Keywords: Nonlinear dynamic response, Porosity, Porous plates, First order shear deformation theory, Stress function.

1. Introduction

Regarding essential advanced properties compared with conventional features such as high-temperature resistance capacity, functionally graded materials (FGMs) have attracted many researchers and scholars worldwide. Functionally graded materials are microscopically inhomogeneous composites usually made by a mixture of metal and ceramic with a volume faction index, which made the material properties of FGM vary continuously through the thickness of the plate from the metal-rich surface to the ceramic-rich surface. By varying the volume fraction index, new genres of FGM with specifically tailored characteristics have been made, which is applicable to various working conditions including mechanical, thermal, or thermo-mechanical loadings in several industries such as aerospace, power plants, and vessels. Therefore, a lot of research has been conducted to investigate these advanced material structures, especially in the domain of dynamic response and vibration characteristics.

In 2013, Wang and Shen [1] employed a two-step perturbation technique to show the nonlinear dynamic response of

sandwich plates with FGM face sheets using the Mori-Tanaka scheme of material distribution resting on the elastic foundation subjected to varies loading conditions. A four-variable refined plate theory along with the higher-order shear deformation plate theory were used by Han et al. [2] to analyze dynamic instability characteristics of S-FGM plates. Hamilton's principle was used and closed-formed solutions were obtained for simply supported plates resting on the elastic foundation under periodic axial excitations. Duy and Noh [3] developed a new refined plate theory based on the classical plate theory by eliminating the shear correction factor to investigate the dynamic response of FGM rectangular plates resting on Pasternak foundation subjected to transverse loadings. Cong et al. [4] presented the nonlinear dynamic response of the eccentrically stiffened FGM plate using Reddy's TSDT in the thermal environment. Hosseini-Hashemi et al. [5] investigated the free vibration of functionally graded rectangular plates using the first-order shear deformation plate theory. Zhao et al. [6] studied the free vibration analysis of functionally graded plates using the element-free kp-Ritz method. More recently, Wang and Zu [7] studied the linear and nonlinear dynamic response of FGM plates moving in the thermal environment by utilizing D'Alembert's principle, Galerkin's method, and the harmonic balance method. The analytical results were verified by numerical studies using an adaptive step-size fourth-order Runge-Kutta technique. Thom et al. [8] studied the analysis of bi-directional functionally graded plates by FEM and a new third-order shear deformation plate theory. Duc et al. [9-13] presented the nonlinear dynamic response and vibration of FGM plates.

In the production progress, porosities might occur in functionally graded structures, therefore, when investigating mechanical, thermal, and thermo-mechanical characteristics of FGM structures, many researchers considered the influences of porosities. In 2005, Piazza et al. [14] conducted experimental studies in disk-shaped samples of piezoceramic material showing the physical and electrical properties in the planar and transverse direction of the disk under the variation of porosity degree. In 2015, Rad and Shariyat [15] utilized 3D theory of elasticity and differential quadrature techniques to analyze porous FGM circular plates with various thicknesses under non-axisymmetric and non-uniform shear and normal tractions and a magnetic actuation resting on the Kerr elastic foundation. Ebrahimi and Zia [16] investigated the nonlinear free vibration of non-homogeneous functionally graded beams with porosities using Timoshenko beam theory, Hamilton's principle, and Galerkin's method. The internal residual stress due to thermal mismatch of ceramic and metal in addition to the effects of residual stress on mechanical performances of porous functionally graded materials are examined by Zhou et al. [17]. Zhou and co-workers [18] also studied the effect of bolt-nut parameters of porous FGM bolted joints under the thermomechanical loading with distributed loads in thread using ABAQUS scripts. The linear and nonlinear vibration behavior of FGM beams having porosities with various kinds of elastic supports were evaluated by Wattanasakulpong and Ungbhakorn [19] using the differential transformation method (DTM). More recently, Ghadiri and SafarPour [20] employed the basis of the first-order shear deformation shells and the modified couple stress theory to study the free vibration behavior of FGM porous cylindrical microshells considering temperature-dependent characteristics in the thermal environment. An experimental and numerical study was carried out by Jahwari and Naguib [21] to analyze plate-like structures of Polylactic Acid whose viscoelastic behavior is assumed to obey Boltzmann superposition principle using the author's newly-developed higher order plate theory. Mechab et al. [22] used the two-variable refined plate theory to evaluate the effect of porosities on porous FGM nano-plate supported by the elastic foundation considering the nonlocal elasticity theory and the Monte Carlo method. Torres et al. [23] developed and characterized samples of titanium with porous functionally radial graded cylinders using bio-inspired and bio-mimetic approaches for potential bone implant applications. Shafiei et al. [24- 26] studied the nonlinear vibration behavior and buckling features of the 2D imperfect functionally graded (2D-FG) tapered Euler-Bernoulli beams in nano- and micro- scales. Barati and Shahverdi [27] dealt with the hygro-thermal divergence and the flutter analysis to investigate the aero-hygro-thermal instability of porous FGM panels under the supersonic airflow using the newly-developed higher-order shear deformation theory. The nonlinear free vibration behavior and post-buckling loads of multilayer functionally graded porous nanocomposite beams that were made of metal foams reinforced by graphene platelets were studied by Chen et al. [28] using Ritz method considering Timoshenko beam theory and von Karman nonlinearity. Ebrahimi et al. [29] proposed a four-variable shear deformation refined plate theory to analyze dynamic responses of embedded smart plates made of magneto-electro-elastic functionally graded materials with porosity resting on the elastic foundation. Şimşek et al. [30] used Mindlin plate theory and the modified couple stress theory to investigate static bending features and forced vibration of an imperfect porous FG microplate with a moving load. Shahverdi and Barati [31] developed a general nonlocal strain-gradient elastic model to study the vibration characteristics of plates with nano-scale porosities supported by an elastic substrate under the hygro-thermal loading. Akbaş [32] employed the first-order shear deformation plate theory along with Hamilton's principle to scrutinize free vibration and static bending responses of a simply supported FG plate in porous phase. Shojaeefard et al. [33] conducted a numerical study analyzing the thermal buckling behavior and free vibration of FG micro-scale porous plate with temperature-dependent properties using CPT, FSDT in conjunction with the modified couple stress theory. Wang et al. [34] studied the steady-state analytical solutions and nonlinear vibrational responses of a longitudinal travelling porous FGM plates and developed a computational model to investigate the vibration behavior of a FG porous cylindrical shell with various boundary conditions using a sinusoidal shear deformation theory and Rayleigh-Ritz method [35]. Ziane et al. [36] presented an analytical study evaluating the critical moment and critical temperature gradients of simply supported and clamped-clamped FGM box beams in the porous phase.

Although various analytical methods have been used to analyze static, dynamic, and vibration behavior of FGM beams, plates, and shells, few studies have been conducted in nonlinear vibration characteristics of FGM plate using the first-order shear deformation theory. This study presented an analytical approach to evaluate natural frequencies and dynamic responses of a simply supported FG plate under a uniform temperature rise and uniform compressive forces using FSDT. Numerical results illustrated the good agreement of the present study with others in the literature and showed the influence of the volume fraction index, porosity degree and types, geometrical configuration, elastic foundations, mechanical loading amplitude, and

uniform temperature rise on nonlinear dynamic responses of the plates.

2. FGM plate with porosities

Consider a plate on elastic foundations. The plate is referred to a Cartesian coordinate system x,y,z, where xy is the mid-plane of the plate and z is the thickness coordinator, $-h/2 \leq z \leq h/2$. The length, width, and total thickness of the plate are a, b, and h, respectively.
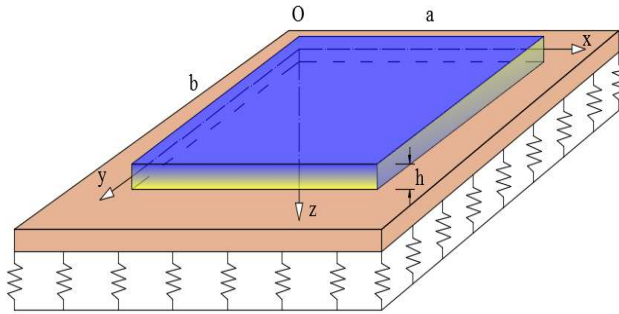
Fig. 1a. Geometry and coordinate system of the FGM plate surrounded on elastic foundations.
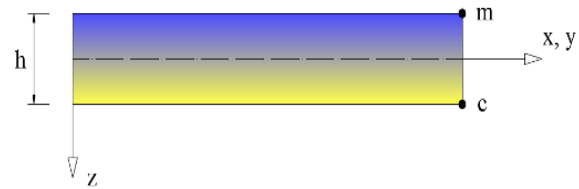
Fig. 1b. Power-law distribution of the FGM plate

The reaction–deflection relation of Pasternak foundation is given by:

$$q_e = K_w w - K_p \nabla^2 w \tag{1}$$

where $\nabla^2 = \partial^2/\partial x^2 + \partial^2/\partial y^2$, w is the deflection of the FGM shell, K_w and K_p are Winkler foundation stiffness and shear layer stiffness of Pasternak foundation, respectively. In this study, two porosity phases are considered including evenly distribution (Porosity-I) and unevenly distribution (Porosity-II) along the plate thickness direction (Fig. 2).
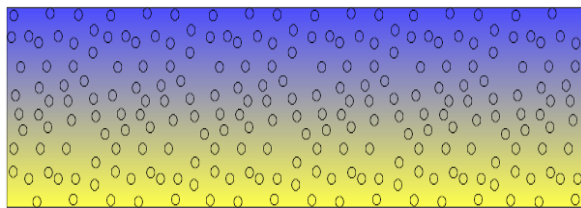
Fig. 2a. Evenly distributed porosities (Porosity – I)
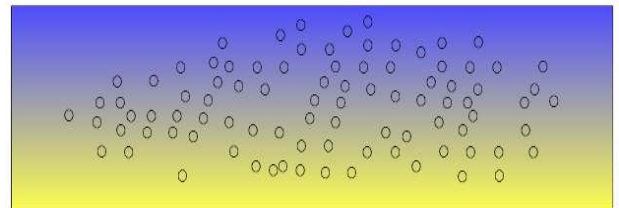
Fig. 2b. Unevenly distributed porosities (Porosity – II)

For a plate made of two different constituent materials, the volume fractions $V_m(z)$ and $V_c(z)$ can be written in the power law distribution (Fig. 1b) as follows [37]:

$$V_c(z) = \left(1 + \frac{2z}{h}\right)^N, V_m(z) = 1 - V_c(z), \tag{2}$$

where N is the power law exponent satisfying $0 \leq N < \infty$. The material properties of P-FGM plates are written as [22,24]

$$P(z) = (P_c - P_m)\left(1 + \frac{2z}{h}\right)^N + P_m - P_{por}, \tag{3}$$

in which, with Porosity-I: $P_{por} = \alpha/2(P_c + P_m)$, Porosity-II: $P_{por} = \alpha/2(1 - 2(|z|/h))(P_c + P_m)$. Accordingly, the effective Young's modulus $E(z)$, thermal expansion coefficient $\beta(z)$, and the mass density $\rho(z)$ of porous FGM plates can be written using Eq. (3) as

Porosity-I:

$$\begin{bmatrix} E(z) \\ \beta(z) \\ \rho(z) \end{bmatrix} = \begin{bmatrix} E_{cm} \\ \beta_{cm} \\ \rho_{cm} \end{bmatrix}\left(1 + \frac{2z}{h}\right)^N + \begin{bmatrix} E_m \\ \beta_m \\ \rho_m \end{bmatrix} - \frac{\alpha}{2}\begin{bmatrix} E_c + E_m \\ \beta_c + \beta_m \\ \rho_c + \rho_m \end{bmatrix}. \tag{4a}$$

Porosity-II:

$$
\begin{bmatrix} E(z) \\ \beta(z) \\ \rho(z) \end{bmatrix} = \begin{bmatrix} E_{cm} \\ \beta_{cm} \\ \rho_{cm} \end{bmatrix} \left(1 + \frac{2z}{h}\right)^N + \begin{bmatrix} E_m \\ \beta_m \\ \rho_m \end{bmatrix} - \frac{\alpha}{2}\left(1 - 2\frac{|z|}{h}\right) \begin{bmatrix} E_c + E_m \\ \beta_c + \beta_m \\ \rho_c + \rho_m \end{bmatrix}.
\tag{4b}
$$

where α is the porosity distribution factor, $E_{cm} = E_c - E_m$, $\beta_{cm} = \beta_c - \beta_m$, $\rho_{cm} = \rho_c - \rho_m$, and the Poisson ratio $v(z)$ is assumed to be constant ($v(z) = v$).

3. Governing equations and boundary conditions

3.1. Governing equations for the plates

In the present study, the first-order shear deformation theory is used to establish the motions, obtain the compatibility equations, and determine the nonlinear dynamic response of the FGM plates. The nonlinear strain-displacement relations using FSDT are [37,38]

$$
\begin{pmatrix} \varepsilon_x \\ \varepsilon_y \\ \gamma_{xy} \end{pmatrix} = \begin{pmatrix} \varepsilon_x^0 \\ \varepsilon_y^0 \\ \gamma_{xy}^0 \end{pmatrix} + z \begin{pmatrix} \chi_x \\ \chi_y \\ \chi_{xy} \end{pmatrix}, \quad \begin{pmatrix} \gamma_{xz} \\ \gamma_{yz} \end{pmatrix} = \begin{pmatrix} \dfrac{\partial w}{\partial x} + \phi_x \\ \dfrac{\partial w}{\partial y} + \phi_y \end{pmatrix},
\tag{5}
$$

with

$$
\begin{pmatrix} \varepsilon_x^0 \\ \varepsilon_y^0 \\ \gamma_{xy}^0 \end{pmatrix} = \begin{pmatrix} \dfrac{\partial u}{\partial x} + \dfrac{1}{2}\left(\dfrac{\partial w}{\partial x}\right)^2 \\ \dfrac{\partial v}{\partial y} + \dfrac{1}{2}\left(\dfrac{\partial w}{\partial y}\right)^2 \\ \dfrac{\partial u}{\partial y} + \dfrac{\partial v}{\partial x} + \dfrac{\partial w}{\partial x}\dfrac{\partial w}{\partial y} \end{pmatrix}, \begin{pmatrix} \chi_x \\ \chi_y \\ \chi_{xy} \end{pmatrix} = \begin{pmatrix} \dfrac{\partial \phi_x}{\partial x} \\ \dfrac{\partial \phi_y}{\partial y} \\ \dfrac{\partial \phi_x}{\partial y} + \dfrac{\partial \phi_y}{\partial x} \end{pmatrix},
\tag{6}
$$

in which ε_x^0 and ε_y^0 are normal strains, γ_{xy}^0 is the shear strain in the middle surface of the plate, and γ_{xz}, γ_{yz} are the transverse shear strains components in the plans xz and yz, respectively. u,v,w are the long x,y, and z axes, respectively. ϕ_x and ϕ_y are the rotation angles of the normal vector around y and x axis. Hooke's law for a plate is defined as follows:

$$
\begin{aligned}
(\sigma_x, \sigma_y) &= \frac{E}{1-v^2}\left[(\varepsilon_x, \varepsilon_y) + v(\varepsilon_y, \varepsilon_x) - (1+v)\beta\Delta T (1,1)\right], \\
(\sigma_{xy}, \sigma_{xz}, \sigma_{yz}) &= \frac{E}{2(1+v)}(\gamma_{xy}, \gamma_{xz}, \gamma_{yz}).
\end{aligned}
\tag{7}
$$

The forces and moments of the plate can be expressed across the plate thickness as

$$
\begin{aligned}
(N_i, M_i) &= \int_{-h/2}^{h/2} \sigma_i (1,z)dz, i = x,y,xy, \\
Q_i &= \kappa \int_{-h/2}^{h/2} \sigma_{iz} dz, i = x,y,
\end{aligned}
\tag{8}
$$

in which $\kappa = 5/6$ is the correction factor. Substituting Eqs. (5) into Eqs. (7) and the result into Eqs. (8) leads to:

$$
\begin{aligned}
(N_x, M_x) &= \frac{1}{1-v^2}\left[(E_1, E_2)(\varepsilon_x^0 + v\varepsilon_y^0) + (E_2, E_3)(\chi_x + v\chi_y) - (1+v)(\Phi_a, \Phi_b)\right], \\
(N_y, M_y) &= \frac{1}{1-v^2}\left[(E_1, E_2)(\varepsilon_y^0 + v\varepsilon_x^0) + (E_2, E_3)(\chi_y + v\chi_x) - (1+v)(\Phi_a, \Phi_b)\right], \\
(N_{xy}, M_{xy}) &= \frac{1}{2(1+v)}\left[(E_1, E_2)\gamma_{xy}^0 + (E_2, E_3)\chi_{xy}\right],
\end{aligned}
\tag{9}
$$

$$\left(Q_x, Q_y\right) = \frac{\kappa E_1}{2\left(1+v\right)}\left(\gamma_{xz}, \gamma_{yz}\right),$$

where

$$E_{i+1} = \int_{-h/2}^{h/2} E(z) z^i dz, \quad \left(i = \overline{0,2}\right),$$

$$\left(\Phi_a, \Phi_b\right) = \int_{-h/2}^{h/2} E(z) \beta(z) \Delta T(1,z) dz.$$

(10)

The motion equations of FGM plates supported by elastic foundations using FSDT are [37, 38]

$$\frac{\partial N_x}{\partial x} + \frac{\partial N_{xy}}{\partial y} = I_0 \frac{\partial^2 u}{\partial t^2} + I_1 \frac{\partial^2 \phi_x}{\partial t^2},$$

(11a)

$$\frac{\partial N_{xy}}{\partial x} + \frac{\partial N_y}{\partial y} = I_0 \frac{\partial^2 v}{\partial t^2} + I_1 \frac{\partial^2 \phi_y}{\partial t^2},$$

(11b)

$$\frac{\partial Q_x}{\partial x} + \frac{\partial Q_y}{\partial y} + N_x \frac{\partial^2 w}{\partial x^2} + 2N_{xy} \frac{\partial^2 w}{\partial x \partial y} + N_y \frac{\partial^2 w}{\partial y^2} - K_w w + K_p \left(\frac{\partial^2 w}{\partial x^2} + \frac{\partial^2 w}{\partial y^2}\right) + q = I_0 \frac{\partial^2 w}{\partial t^2},$$

(11c)

$$\frac{\partial M_x}{\partial x} + \frac{\partial M_{xy}}{\partial y} - Q_x = I_2 \frac{\partial^2 \phi_x}{\partial t^2} + I_1 \frac{\partial^2 u}{\partial t^2},$$

(11d)

$$\frac{\partial M_{xy}}{\partial x} + \frac{\partial M_y}{\partial y} - Q_y = I_2 \frac{\partial^2 \phi_y}{\partial t^2} + I_1 \frac{\partial^2 v}{\partial t^2},$$

(11e)

where q is an external pressure uniformly distributed on the surface of the plate and

$$I_i = \int_{-h/2}^{h/2} \rho(z) z^i dz, \quad \left(i = \overline{0,2}\right).$$

(12)

The stress function $f(x,y,t)$ is introduced as

$$N_x = \frac{\partial^2 f}{\partial y^2}, N_y = \frac{\partial^2 f}{\partial x^2}, N_{xy} = -\frac{\partial^2 f}{\partial x \partial y}.$$

(13)

The reverse relations are obtained from Eqs. (9) as

$$\varepsilon_x^0 = \frac{1}{E_1}\left[\frac{\partial^2 f}{\partial y^2} - v\frac{\partial^2 f}{\partial x^2} - E_2 \frac{\partial \phi_x}{\partial x} + \Phi_a\right], \varepsilon_y^0 = \frac{1}{E_1}\left[\frac{\partial^2 f}{\partial x^2} - v\frac{\partial^2 f}{\partial y^2} - E_2 \frac{\partial \phi_y}{\partial y} + \Phi_a\right],$$

$$\gamma_{xy}^0 = -\frac{1}{E_1}\left[2(1+v)\frac{\partial^2 f}{\partial x \partial y} + E_2 \frac{\partial \phi_x}{\partial y} + E_2 \frac{\partial \phi_y}{\partial x}\right].$$

(14)

Replacing Eq. (13) into Eqs. (11a) and (11b) yields

$$\frac{\partial^2 u}{\partial t^2} = -\frac{I_1}{I_0}\frac{\partial^2 \phi_x}{\partial t^2},$$

(15a)

$$\frac{\partial^2 v}{\partial t^2} = -\frac{I_1}{I_o}\frac{\partial^2 \phi_y}{\partial t^2}.$$

(15b)

By substituting Eqs. (13) and (15) into Eqs. (11c-11e), it can be rewritten as follows:

$$\frac{\partial Q_x}{\partial x} + \frac{\partial Q_y}{\partial y} + \frac{\partial^2 f}{\partial y^2}\frac{\partial^2 w}{\partial x^2} - 2\frac{\partial^2 f}{\partial x \partial y}\frac{\partial^2 w}{\partial x \partial y} + \frac{\partial^2 f}{\partial x^2}\frac{\partial^2 w}{\partial y^2} - K_w w + K_p \left(\frac{\partial^2 w}{\partial x^2} + \frac{\partial^2 w}{\partial y^2}\right) + q = \rho_0 \frac{\partial^2 w}{\partial t^2},$$

(16a)

$$\frac{\partial M_x}{\partial x} + \frac{\partial M_{xy}}{\partial y} - Q_x = \left(I_2 - \frac{I_1^2}{I_0}\right)\frac{\partial^2 \phi_x}{\partial t^2},$$

(16b)

$$\frac{\partial M_{xy}}{\partial x} + \frac{\partial M_y}{\partial y} - Q_y = \left(I_2 - \frac{I_1^2}{I_o}\right)\frac{\partial^2 \phi_y}{\partial t^2}.$$

(16c)

The deformation compatibility equation for FGM plates can be written as

$$\frac{\partial^2 \varepsilon_x^0}{\partial y^2} + \frac{\partial^2 \varepsilon_y^0}{\partial x^2} - \frac{\partial^2 \gamma_{xy}^0}{\partial x \partial y} = \left(\frac{\partial^2 w}{\partial x \partial y}\right)^2 - \frac{\partial^2 w}{\partial x^2}\frac{\partial^2 w}{\partial y^2}. \tag{17}$$

Substitution of Eqs. (14) into the deformation compatibility equation (17) leads to

$$\frac{1}{E_1}\left(\frac{\partial^4 f}{\partial x^4} + 2\frac{\partial^4 f}{\partial x^2 \partial y^2} + \frac{\partial^4 f}{\partial y^4}\right) = \left(\frac{\partial^2 w}{\partial x \partial y}\right)^2 - \frac{\partial^2 w}{\partial x^2}\frac{\partial^2 w}{\partial y^2}. \tag{18}$$

By substituting Eq. (9) into Eqs. (16), the system of motion in Eqs. (16) is rewritten as follows:

$$\begin{bmatrix} H_{11} & H_{12} & H_{13} \\ H_{21} & H_{22} & H_{23} \\ H_{31} & H_{32} & H_{33} \end{bmatrix}\begin{bmatrix} w \\ \phi_x \\ \phi_y \end{bmatrix} + \begin{bmatrix} P(w,f) \\ 0 \\ 0 \end{bmatrix} + \begin{bmatrix} q \\ 0 \\ 0 \end{bmatrix} = \begin{bmatrix} \rho_o & 0 & 0 \\ 0 & \rho_1 & 0 \\ 0 & 0 & \rho_1 \end{bmatrix}\begin{bmatrix} \dfrac{\partial^2 w}{\partial t^2} \\[2mm] \dfrac{\partial^2 \phi_x}{\partial t^2} \\[2mm] \dfrac{\partial^2 \phi_y}{\partial t^2} \end{bmatrix}, \tag{19}$$

where $H_{ij}\left(i=\overline{1,3}, j=\overline{1,3}\right)$, $\rho_q\left(q=\overline{0,1}\right)$ and the nonlinear operator P is shown in Appendix I. Boundary conditions and initial conditions along with Eqs. (18) and (19) are used for the nonlinear dynamic analysis of porous FGM plates.

3.2. Boundary conditions

In this study, the FGM plates are assumed to be simply supported. Two boundary conditions, labeled as Case I and Case II, are considered [4, 37].

Case I: Four edges of the plate are simply supported and freely movable (FM):

$$\begin{aligned} w = N_{xy} = \phi_y = M_x = 0, N_x = N_{x0} \quad at \quad x = 0, a, \\ w = N_{xy} = \phi_x = M_y = 0, N_y = N_{y0} \quad at \quad y = 0, b. \end{aligned} \tag{20}$$

Case II: Four edges of the plate are simply supported and immovable (IM):

$$\begin{aligned} w = u = \phi_y = M_x = 0, N_x = N_{x0} \quad at \quad x = 0, a, \\ w = v = \phi_x = M_y = 0, N_y = N_{y0} \quad at \quad y = 0, b. \end{aligned} \tag{21}$$

in which N_{x0}, N_{y0} are pre-buckling compressive force resultants in x, y directions, respectively (FM), and are the jets when the edges are immovable in the plane of the plate (IM). The approximate solutions of the system of Eqs. (16) and (17) by satisfying the boundary conditions (20, 21) can be written as

$$\begin{aligned} w(x,y,t) &= W(t)\sin(\lambda_m x)\sin(\beta_n y), \\ \phi_x(x,y,t) &= \Phi_x(t)\cos(\lambda_m x)\sin(\beta_n y), \\ \phi_y(x,y,t) &= \Phi_y(t)\sin(\lambda_m x)\cos(\beta_n y), \end{aligned} \tag{22a}$$

$$f(x,y,t) = A_1(t)\cos(2\lambda_m x) + A_2(t)\cos(2\beta_n y) + \frac{1}{2}N_{x0}y^2 + \frac{1}{2}N_{y0}x^2, \tag{22b}$$

where $\lambda_m = \dfrac{m\pi}{a}, \beta_n = \dfrac{n\pi}{b}$, W, Φ_x, Φ_y - the amplitudes which are dependent-on-time functions. The coefficients $A_i(i=1-2)$ are determined as

$$A_1 = \frac{E_1\beta_n^2}{32\lambda_m^2}W^2, A_2 = \frac{E_1\lambda_m^2}{32\beta_n^2}W^2. \tag{22c}$$

Replacing Eq. (22) into the equations of motion (19) and then applying Galerkin method leads to

$$\begin{bmatrix} h_{11}+n_2 N_{x0}+n_4 N_{y0} & h_{12} & h_{13} \\ h_{21} & h_{22} & h_{23} \\ h_{31} & h_{32} & h_{33} \end{bmatrix}\begin{bmatrix} W \\ \Phi_x \\ \Phi_y \end{bmatrix} + n_1\begin{bmatrix} W^3 \\ 0 \\ 0 \end{bmatrix} + n_3\begin{bmatrix} q \\ 0 \\ 0 \end{bmatrix} = \begin{bmatrix} \rho_o & 0 & 0 \\ 0 & \rho_1 & 0 \\ 0 & 0 & \rho_1 \end{bmatrix}\begin{bmatrix} \dfrac{\partial^2 W}{\partial t^2} \\[2mm] \dfrac{\partial^2 \Phi_x}{\partial t^2} \\[2mm] \dfrac{\partial^2 \Phi_y}{\partial t^2} \end{bmatrix}, \tag{23}$$

while the coefficients $h_{ij}\left(i=\overline{1,3}\,j=\overline{1,3}\right),n_q\left(q=\overline{1,3}\right)$ are shown in Appendix II.

3.3. Nonlinear dynamic analysis of FGM plates subjected to the mechanical load

Consider a simply supported and freely movable FGM plate (FM - Case I of boundary conditions). Assume that the FGM plate is loaded under uniform compressive forces P_x and P_y (Pascal) on the edges $x=0,a$, and $y=0,b$

$$N_{x0}=-P_x\,h,\ N_{y0}=-P_y\,h. \tag{24}$$

Substituting Eq. (24) into Eq. (23) leads to the system of equations for studying the nonlinear dynamic response of the FGM plates as follows:

$$\begin{bmatrix} h_{11}-\left(n_2P_x+n_4P_y\right)h & h_{12} & h_{13}\\ h_{21} & h_{22} & h_{23}\\ h_{31} & h_{32} & h_{33}\end{bmatrix}\begin{bmatrix}W\\ \Phi_x\\ \Phi_y\end{bmatrix}+n_1\begin{bmatrix}W^3\\0\\0\end{bmatrix}+n_3\begin{bmatrix}q\\0\\0\end{bmatrix}=\begin{bmatrix}\rho_o & 0 & 0\\0 & \rho_1 & 0\\0 & 0 & \rho_1\end{bmatrix}\begin{bmatrix}\dfrac{\partial^2 W}{\partial t^2}\\[6pt]\dfrac{\partial^2\Phi_x}{\partial t^2}\\[6pt]\dfrac{\partial^2\Phi_y}{\partial t^2}\end{bmatrix}. \tag{25}$$

The natural frequencies of the plate without load q can be determined directly by solving the determinant derived from Eqs. (25) after eliminating all nonlinear components as

$$\begin{vmatrix} h_{11}-\left(n_2P_x+n_4P_y\right)h+I_0\omega^2 & h_{12} & h_{13}\\ h_{21} & h_{22}+\rho_1\omega^2 & h_{23}\\ h_{31} & h_{32} & h_{33}+\rho_1\omega^2\end{vmatrix}=0. \tag{26}$$

3.4. Nonlinear dynamic analysis of FGM plates subjected to the thermal load

Consider a simply supported and immovable FGM plate (FM - Case II of boundary conditions) under the thermal load. The condition expressing the immovability on the edges, $u=0$ (at $x=0,a$), and $v=0$ (at $y=0,b$) is satisfied in an average sense as [37]

$$\int_0^b\int_0^a\frac{\partial u}{\partial x}dxdy=0,\ \int_0^a\int_0^b\frac{\partial v}{\partial y}dxdy=0. \tag{27}$$

From Eqs. (5) and (14) one can obtain the following expression:

$$\frac{\partial u}{\partial x}=\frac{1}{E_1}\left(\frac{\partial^2 f}{\partial y^2}-v\frac{\partial^2 f}{\partial x^2}\right)-\frac{E_2}{E_1}\frac{\partial\phi_x}{\partial x}-\frac{1}{2}\left(\frac{\partial w}{\partial x}\right)^2+\frac{\Phi_a}{E_1},$$

$$\frac{\partial v}{\partial y}=\frac{1}{E_1}\left(\frac{\partial^2 f}{\partial x^2}-v\frac{\partial^2 f}{\partial y^2}\right)-\frac{E_2}{E_1}\frac{\partial\phi_y}{\partial y}-\frac{1}{2}\left(\frac{\partial w}{\partial y}\right)^2+\frac{\Phi_a}{E_1}. \tag{28}$$

Substitution of Eqs. (22) into Eq. (28) and then the results into Eq. (27) yields

$$N_{x0}=-\frac{\Phi_a}{1-v}-\frac{4E_2}{mn\pi^2\left(1-v^2\right)}\left(\frac{m\pi}{a}\Phi_x+v\,\Phi_y\frac{n\pi}{b}\right)+\frac{E_1}{8\left(1-v^2\right)}\left[v\left(\frac{n\pi}{b}\right)^2+\left(\frac{m\pi}{a}\right)^2\right]W^2,$$

$$N_{y0}=-\frac{\Phi_a}{1-v}-\frac{4E_2}{mn\pi^2\left(1-v^2\right)}\left(v\frac{m\pi}{a}\Phi_x+\frac{n\pi}{b}\Phi_y\right)+\frac{E_1}{8\left(1-v^2\right)}\left[v\left(\frac{m\pi}{a}\right)^2+\left(\frac{n\pi}{b}\right)^2\right]W^2, \tag{29}$$

where $\Phi_a=P\Delta T$ with $P=\displaystyle\int_{-h/2}^{h/2}E\left(z\right)\beta\left(z\right)dz$. By substituting Eqs. (29) into Eqs. (23), the basic equations used to investigate the nonlinear dynamic response of the FGM plates in the Case II of boundary condition as follows:

$$\left(h_{11} - \left(n_2 + n_4\right)\frac{P\Delta T}{1-v}\right)W + h_{12}\Phi_x + h_{13}\Phi_y + h_{14}\Phi_x W + h_{15}\Phi_y W + h_{16}W^3 + n_3 q = \rho_o \frac{\partial^2 W}{\partial t^2},$$

$$h_{21}W + h_{22}\Phi_x + h_{23}\Phi_y = \rho_1 \frac{\partial^2 \Phi_x}{\partial t^2}, \qquad (30)$$

$$h_{31}W + h_{32}\Phi_x + h_{33}\Phi_y = \rho_1 \frac{\partial^2 \Phi_y}{\partial t^2},$$

while the coefficients $h_{ij}\left(i=1, j=\overline{4,6}\right)$ are shown in Appendix II. The natural frequencies of the plate without load q can be determined directly by solving the determinant derived from Eqs. (30) after eliminating all nonlinear components:

$$\begin{vmatrix} h_{11} - \left(n_2 + n_4\right)\dfrac{P\Delta T}{1-v} + I_0\omega^2 & h_{12} & h_{13} \\ h_{21} & h_{22} + \rho_1\omega^2 & h_{23} \\ h_{31} & h_{32} & h_{33} + \rho_1\omega^2 \end{vmatrix} = 0. \qquad (31)$$

4. Numerical results and discussion

This study investigates a porous FGM plates in the presence of an excited force $q = Q\sin\Omega t$. Q is amplitude of the excited force and Ω is frequency of the force. Numerical results for the dynamic response of porous FGM plates are obtained by Runge–Kutta method. Consider a FGM plate with effective material properties as shown in Table 1 [37].

Table 1. Properties of the functionally graded material components.

Material	Properties			
	E (GPa)	v	$\alpha\left(/^0 C\right)$	$\rho\left(kg/m^3\right)$
Aluminum $\left(Al\right)$	70	0.3	23×10^{-6}	2702
Alumina $\left(Al_2O_3\right)$	380	0.3	7.4×10^{-6}	3800

4.1. Validation

In order to check the reliability of the method used in this paper, the value of the fundamental frequency parameter $\omega_N = \omega h\sqrt{\rho_c / E_c}$ of FGM plates without elastic foundations is compared with results of Ref [5, 6] and the comparison on dynamic responses is made with results of Ref [12]. Table 2 shows the influence of volume fraction index N and thickness to length ratio $\left(h/a\right)$ on the fundamental frequency of the FGM plates. The geometrical parameters for the FGM plates are chosen as $a/b = 1, (m, n) = (1,1), P_x = 0, P_y = 0, \Delta T = 0$. As can be seen in this table, the values of fundamental frequency show a significant difference and a good agreement is obtained in this comparison.

Table 2. Comparison of fundamental frequency parameter $\omega_N = \omega h\sqrt{\rho_c / E_c}$ of FGM plates

N	$h/a = 0.05$			$h/a = 0.1$			$h/a = 0.2$		
	Ref [5]	Ref [6]	Present	Ref [5]	Ref [6]	Present	Ref [5]	Ref [6]	Present
0	0.0148 0%	0.0146 1.35%	0.0148	0.0577 0%	0.0567 1.73%	0.0577	0.2112 0%	0.2055 2.70%	0.2112
0.5	0.0128 2.4%	0.0124 0.8%	0.0125	0.0492 0.41%	0.0482 1.63%	0.0490	0.1806 0%	0.1757 2.71%	0.1806
1	0.0115 1.77%	0.0112 0.89%	0.0113	0.0445 0.68%	0.0435 1.58%	0.0442	0.1650 0.98%	0.1587 2.88%	0.1634
10	0.0096 2.13%	0.0093 1.06%	0.0094	0.0363 0.82%	0.0359 1.91%	0.0366	0.1304 1.81%	0.1284 3.13%	0.1328

Figure 3 indicates the comparison of the dynamic response of P-FGM plates without elastic foundations and with the same geometrical parameters.
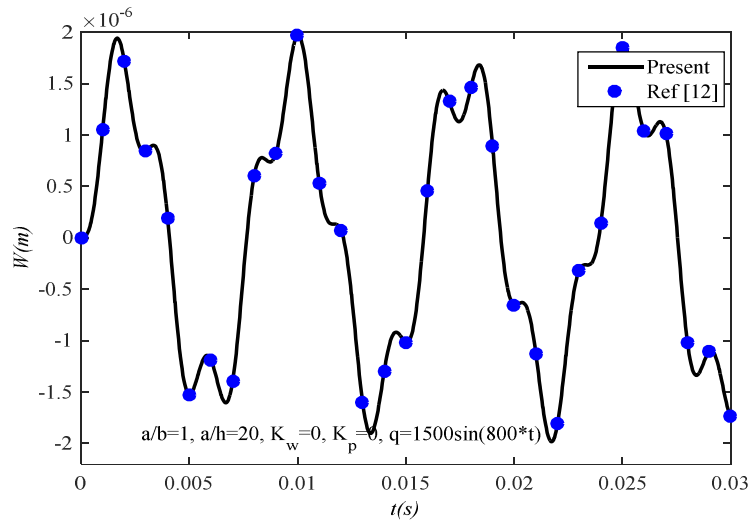
Fig. 3. The comparison of the dynamic response of P-FGM plates

4.2. The natural frequency and dynamic response of the porous FGM plates

Table 3 shows the influence of the porosity volume fraction and the volume faction index on the natural frequencies of porous FGM plates. As can be noticed in this table, when the value of the porosity volume fraction and the volume faction index increase, the stiffness of porous FGM plates and the values of natural frequency decreases, and vice versa. The values of natural frequencies of Porosity-II type is consistently higher than that of Porosity-I type.

Table 3. Effect of the porosity volume fraction and the volume faction index on the natural frequencies $\left(s^{-1}\times 10^{3}\right)$ of porous FGM plates with $a/b = 1, a/h = 20, P_x = 0, P_y = 0, K_w = 0, K_p = 0.$

	N	0.5	1	3	5	10
	$\alpha = 0$	2.5139	2.2663	1.9951	1.9518	1.8885
Porosity-I	$\alpha = 0.1$	2.5095	2.2164	1.8606	1.8061	1.7494
	$\alpha = 0.2$	2.5021	2.1445	1.6330	1.5426	1.4936
	$\alpha = 0$	2.5139	2.2663	1.9951	1.9518	1.8885
Porosity-II	$\alpha = 0.1$	2.5416	2.2785	1.9799	1.9348	1.8771
	$\alpha = 0.2$	2.5715	2.2907	1.9573	1.9086	1.8579

Figure 4 illustrates the effect of the volume fraction index $N = 0, 1, 3$ on the nonlinear dynamic response of porous FGM plates. As can be seen in the figure, the amplitude of the nonlinear dynamic response of FGM porous plate increases proportionally with the volume fraction index. It is obvious that by raising the value of N in Eq. (2), the volume of metal increases while the volume of ceramic decreases which leads to the reduction of plate stiffness.
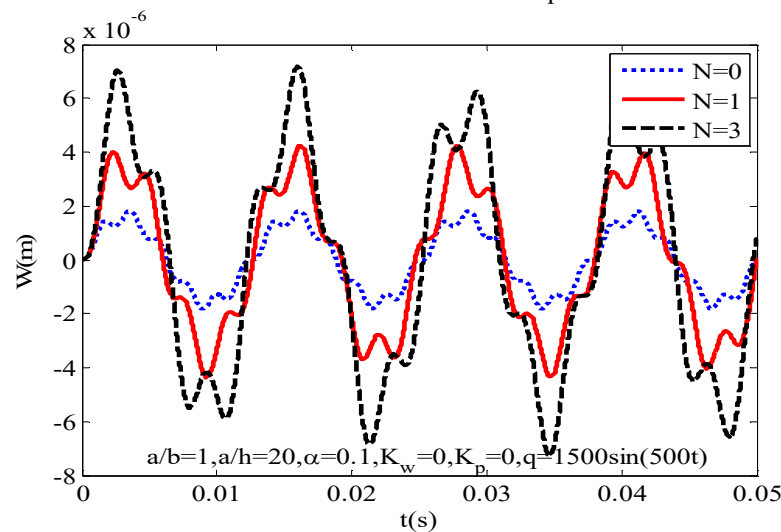
Fig. 4. Nonlinear dynamic response of porous FGM plates with various volume faction index N.

Figures 5 and 6 show the effect of the porosity volume fraction (α) with variously distributed types. Three sets of porosity volume factions are considered, $\alpha = (0, 0.1, 0.2)$. As can be observed in these figures, the higher the porosity volume fraction α, the higher the amplitude of FGM plates. Moreover, the amplitude of FGM plate in Porosity-I phase is higher than

that in Porosity-II phase.
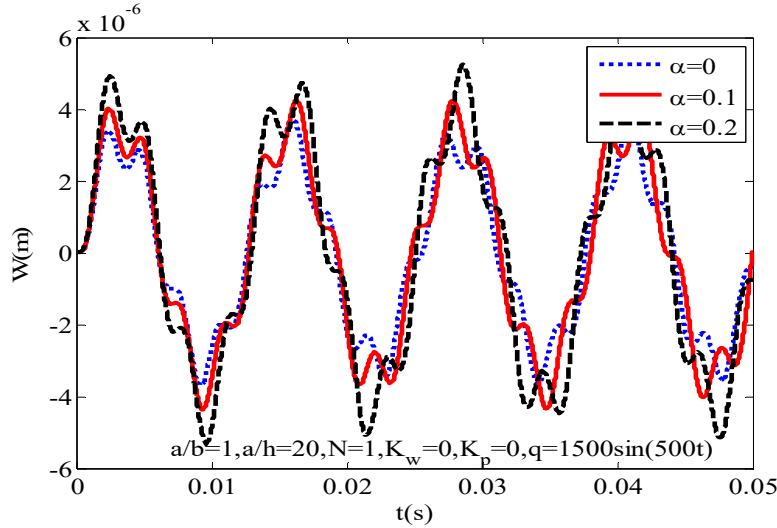
Fig. 5. Effect of the porosity volume fraction α of Porosity-I on the nonlinear dynamic response of FGM plates.
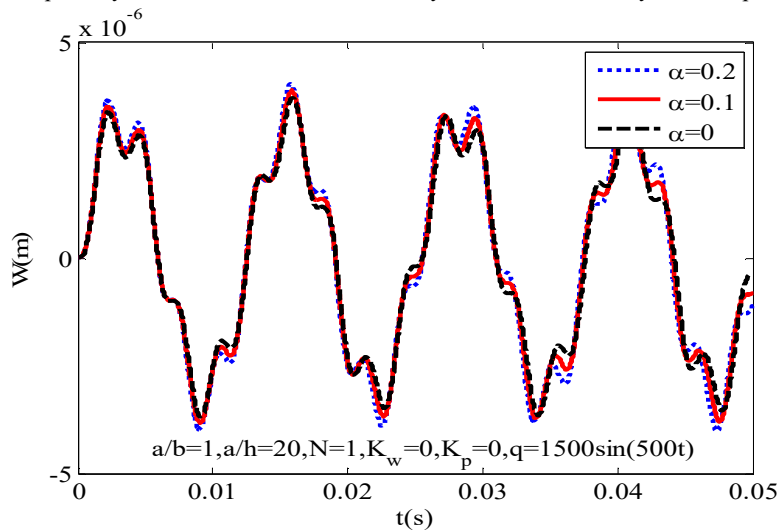
Fig. 6. Effect of the porosity volume fraction α of Porosity-II on the nonlinear dynamic response of FGM plates.

Figures 7 and 8 show the influence of geometric parameters on the nonlinear dynamic response of FGM porous plate in Case I of boundary condition. In Fig. 7, the value of parameter a and the change value of parameter b are fixed. It can be seen that the amplitude of the dynamic response decreases when rising length to width ratio (a/b).

It is obvious in Fig. 8 that porous FGM plates have significant fluctuation when length to thickness ratio (a/h) of the plate is observed. It is also understood that a/h increase makes porous FGM plates thinner which results in the lower load capacity of porous FGM plates.
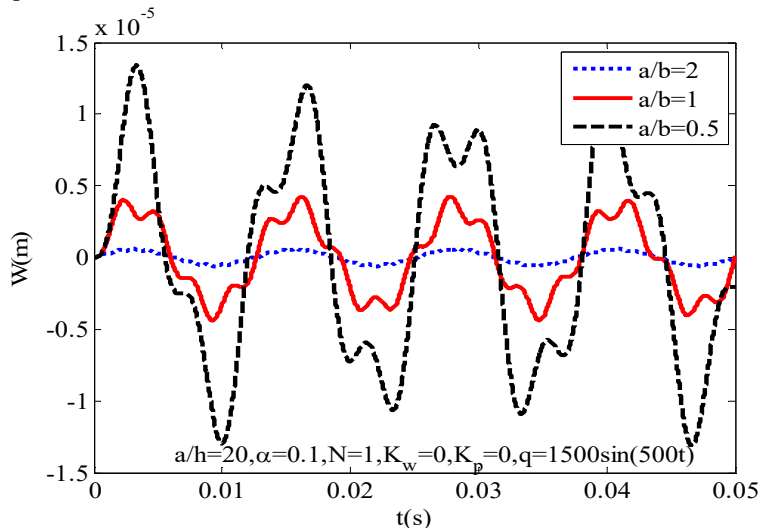
Fig. 7. Effect of length to width ratio a/b on the nonlinear dynamic response of porous FGM plates.
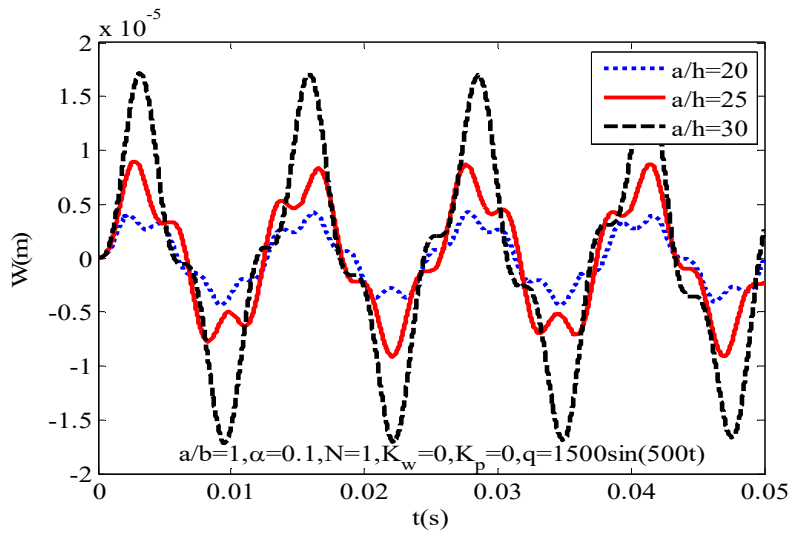
Fig. 8. Effect of length to thickness ratio a/h on the nonlinear dynamic response of porous FGM plates.

Figures 9 and 10 show the effect of linear Winkler and Pasternak foundations K_w, K_p stiffness on the dynamic response of the plate. Considering porous FGM plates (Porosity-I) in the Case I of boundary condition, the amplitude of porous FGM plates increases when the modulus of elastic foundation decreases. In addition, the Pasternak type elastic foundation with the coefficient K_p has a significant effect compared with the Winkler type elastic foundation on the plate dynamic behavior.
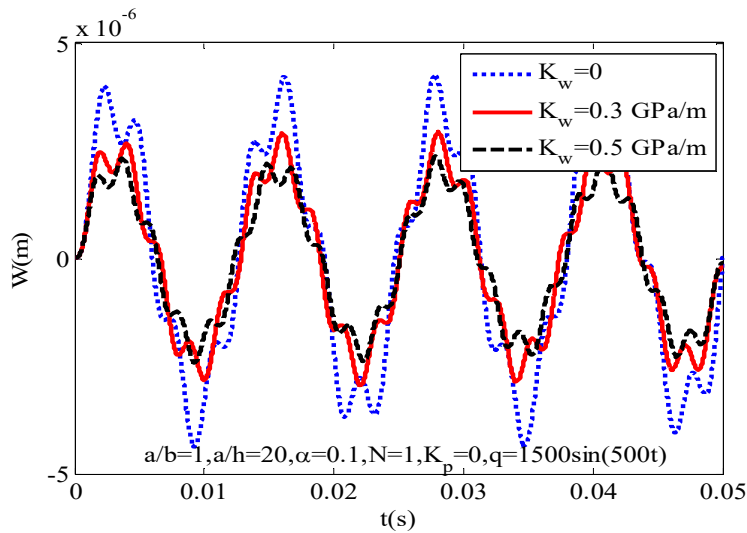
Fig. 9. Effect of the Winkler modulus parameter K_w on the dynamic response of porous FGM plates.
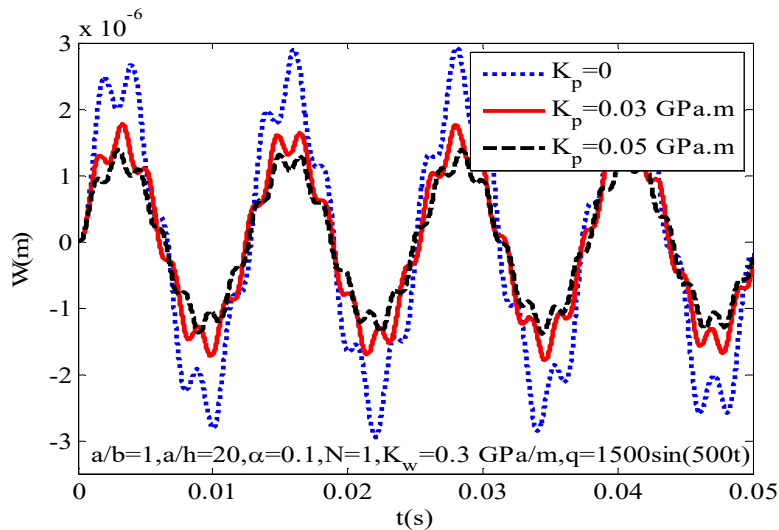
Fig. 10. Effect of the Pasternak modulus parameter K_p on the dynamic response of porous FGM plates.

Figure 11 presents the influence of excited force amplitude on the nonlinear dynamic response of porous FGM plates in

three cases of the excitation force amplitude $Q = \left(1500, 2000, 2500\, N\,/\,m^2\right)$. Clearly, when Q decreases, the amplitude of plates decreases as well. Figure 12 illustrates the effect of pre-loaded axial compression P_x on the nonlinear dynamic response of porous FGM plates. It can be seen in this figure, the value of the amplitude of porous FGM plates decreases when the value of axial compressive force P_x decreases.
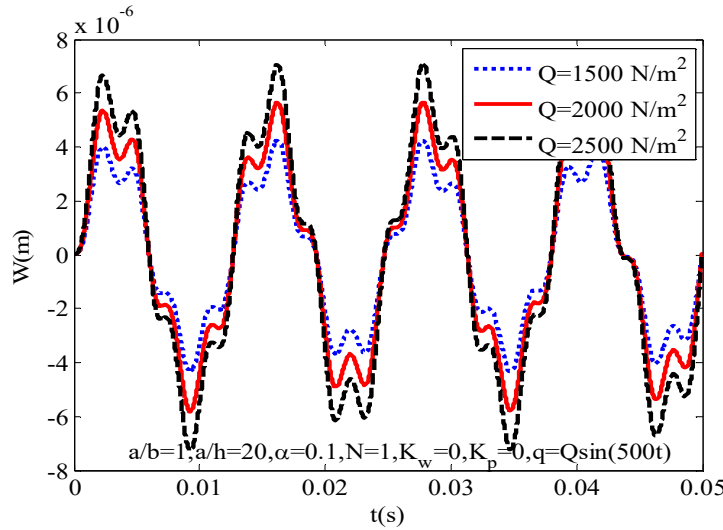
Fig. 11. Effect of amplitude Q on the dynamic response of porous FGM plates.
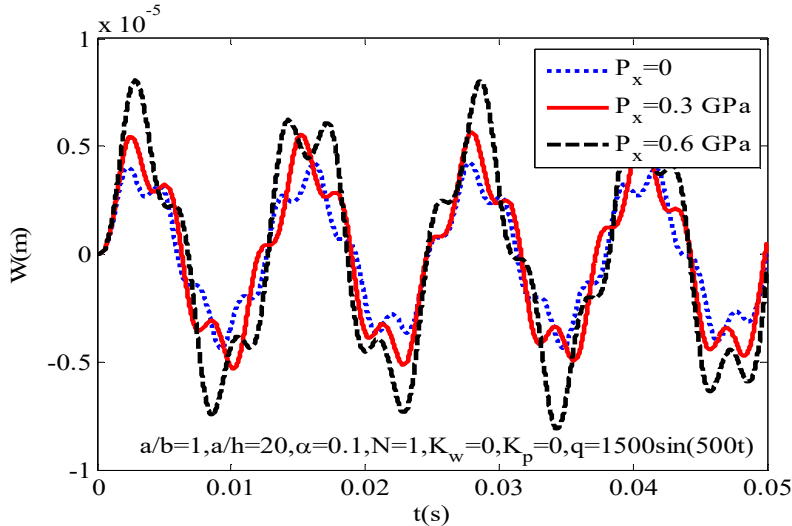
Fig. 12. Effect of pre-loaded axial P_x compression on the dynamic response of porous FGM plates.

Figure 13 shows the effect of temperature increment $\Delta T = \left(0, 50, 100\right)(K)$ on the nonlinear dynamic response of porous FGM plates in Case II of boundary condition. The value of amplitude decreases when the temperature ΔT decreases. In other words, the temperature field has a negative effect on the dynamic response of porous FGM plates.

5. Conclusions

This paper investigates the nonlinear dynamic response of porous FGM plates on the elastic foundation based on the first order shear deformation theory and Airy stress function. Numerical results for the dynamic response of porous FGM plates are obtained using Runge-Kutta method. The conclusions obtained from this study are as follows:

- The value of the amplitude and natural frequency of FGM plates is effected by various distribution of porosity. The value of the amplitude of FGM plates in Porosity-I phase is higher than that in Porosity-II phase. However, the value of the natural frequency of FGM plates in the case Porosity-I is lower than the other.
- The time-amplitude response curves of porous FGM plates are obtained and the influences of geometrical parameters, elastic foundations, excitation force, and mechanical as well as thermal loads on the nonlinear dynamic response of porous FGM plates are examined.
- The temperature field has a significant effect on the nonlinear dynamic response of porous FGM plates. On the other hand, the temperature increment has a negative effect on the amplitudes of porous FGM plates.
- The results of the present study are compared with that of other studies by using methods to validate the reliability of the corresponding method used in this research.
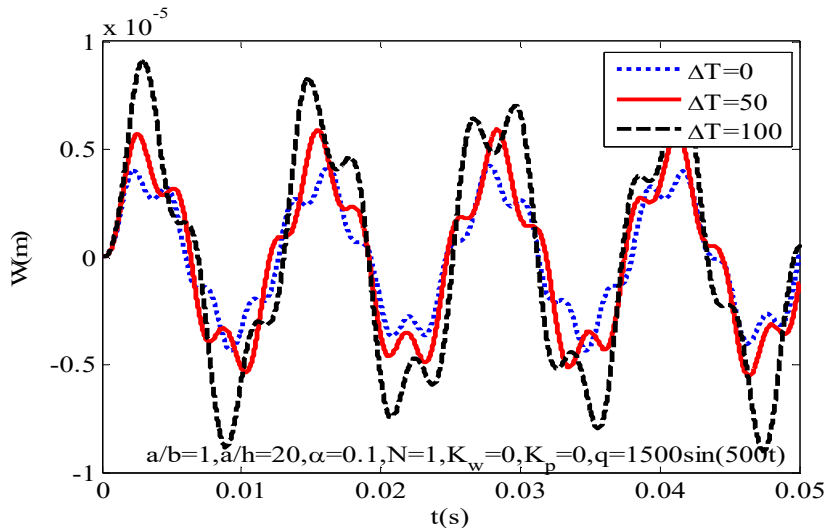
Fig. 13. Effect of temperature on the nonlinear response of porous FGM plates.

References

[1] Wang, Z.X., Shen, H.S., Nonlinear dynamic response of sandwich plates with FGM face sheets resting on elastic foundations in thermal environments, *Ocean Engineering*, 57, 2013, 99–110.

[2] Han, S.C., Park, W.T., Jung, W.Y., A four-variable refined plate theory for dynamic stability analysis of S-FGM plates based on physical neutral surface, *Composite Structures*, 131, 2015, 1081-1089.

[3] Duy, H.T., Noh, H.C., Analytical solution for the dynamic response of functionally graded rectangular plates resting on elastic foundation using a refined plate theory, *Applied Mathematical Modelling*, 39(20), 2015, 6243-6257.

[4] Cong, P.H., Anh, V.M., Duc, N.D., Nonlinear dynamic response of eccentrically stiffened FGM plate using Reddy's TSDT in thermal environment, *Journal of Thermal Stresses*, 40(6), 2016, 704-732.

[5] Hosseini-Hashemi, Sh., Rokni Damavandi Taher, H., Akhavan, H., Omidi, M., Free vibration of functionally graded rectangular plates using first-order shear deformation plate theory, *Applied Mathematical Modelling*, 34, 2010, 1276-1291.

[6] Zhao, X., Lee, Y.Y., Liew, K.M., Free vibration analysis of functionally graded plates using the element-free kp-Ritz method, *Journal of Sound and Vibration*, 319, 2009, 918-939.

[7] Wang, Y.Q., Zu, J.W., Nonlinear dynamic thermoelastic response of rectangular FGM plates with longitudinal velocity, *Composites Part B*, 117 2017, 74-88.

[8] Thom, D.V., Kien, N.D., Duc, N.D., Duc, H.D., Tinh, Q.B., Analysis of bi-directional functionally graded plates by FEM and a new third-order shear deformation plate theory, *Thin-Walled Structures*, 119, 2017, 687–699.

[9] Duc, N.D., Tuan, N.D., Tran, P., Quan, T.Q., Nonlinear dynamic response and vibration of imperfect shear deformable functionally graded plates subjected to blast and thermal loads, *Mechanics of Advanced Materials and Structures*, 24(4), 2017, 318-329.

[10] Duc, N.D., Cong, P.H., Tuan, N.D., Tran, P., Anh, V.M, Quang, V.D., Nonlinear vibration and dynamic response of imperfect eccentrically stiffened shear deformable sandwich plate with functionally graded material in thermal environment, *Journal of Sandwich Structures and Materials*, 18(4), 2016, 445-473.

[11] Duc, N.D., Cong, P.H., Nonlinear dynamic response of imperfect symmetric thin S-FGM plate with metal-ceramic-metal layers on elastic foundation, *Journal of Vibration and Control*, 21(4), 2015, 637-646.

[12] Duc, N.D., Cong, P.H., Nonlinear vibration of thick FGM plates on elastic foundation subjected to thermal and mechanical loads using the first-order shear deformation plate theory, *Cogent Engineering*, 2, 2015, 1045222.

[13] Duc, N.D., Cong, P.H., Quang, V.D., Thermal stability of eccentrically stiffened FGM plate on elastic foundation based on Reddy's third-order shear deformation plate theory, *Thermal Stresses*, 39(7), 2016, 772-794.

[14] Piazza, D., Capiani, C., Galassi, C., Piezoceramic material with anisotropic graded porosity, *Journal of the European Ceramic Society*, 25, 2005, 3075–3078.

[15] Rad, A.B., Shariyat, M., Three-dimensional magneto-elastic analysis of asymmetric variable thickness porous FGM circular plates with non-uniform tractions and Kerr elastic foundations, *Composite Structures*, 125, 2015, 558-574.

[16] Ebrahimi, F., Zia, M., Large amplitude nonlinear vibration analysis of functionally graded Timoshenko beams with porosities, *Acta Astronautica*, 116, 2015, 117-125.

[17] Zhou, W., Zhou, H., Zhang, R., Pei, Y., Fang, D., Measuring residual stress and its influence on properties of porous ZrO2/(ZrO2+Ni) ceramics, *Materials Science & Engineering A*, 622, 2015, 82–90.

[18] Zhou, W., Zhang, R., Ai, S., He, R., Pei, Y., Fang, D., Load distribution in threads of porous metal–ceramic functionally graded composite joints subjected to thermomechanical loading, *Composite Structures*, 134, 2015, 680–688.

[19] Wattanasakulpong, N., Ungbhakorn, V., Nonlinear vibration of a coating-FGM-substrate cylindrical panel subjected to a temperature gradient, *Computer Methods in Applied Mechanics and Engineering*, 195, 2006, 007-1026.

[20] Ghadiri, M., SafarPour, H., Free vibration analysis of size-dependent functionally graded porous cylindrical microshells in thermal environment, *Journal of Thermal Stresses*, 40, 2017, 55-71.

[21] Jahwari, F. A., Naguib, H. E., Analysis and Homogenization of Functionally Graded Viscoelastic Porous Structures with a Higher Order Plate Theory and Statistical Based Model of Cellular Distribution, *Applied Mathematical Modelling*, 40(3), 2015, 2190-2205.

[22] Mechab, B., Mechab, I., Benaissa, S., Ameri, M., Serier, B., Probabilistic analysis of effect of the porosities in functionally graded material nanoplate resting on Winkler–Pasternak elastic foundations, *Applied Mathematical Modelling*, 40, 2015, 1–12.

[23] Torres, Y., Trueba, P., Pavon, J.J., Chicardi, E., Kamm, P., Garcıa-Moreno, F., Rodrıguez-Ortiz, J.A., Design, processing and characterization of titanium with radial graded porosity for bone implants, *Materials & Design*, 110, 2016, 179-187.

[24] Shafei, N., Mousavi, A., Ghadiri, M., On size-dependent nonlinear vibration of porous and imperfect functionally graded tapered microbeams, *International Journal of Engineering Science*, 106, 2016, 42–56.

[25] Shafei, N., Kazemi, M., Buckling analysis on the bi-dimensional functionally graded porous tapered nano-/ micro-scale beams, *Aerospace Science and Technology*, 66, 2017, 1-11.

[26] Shafei, N., Mirjavadi, S.S., MohaselAfshari, B., Rabbly, S., Kazemi, M., Vibration of two-dimensional imperfect functionally graded (2D-FG) porous nano-/micro-beams, *Computer Methods in Applied Mechanics and Engineering*, 322, 2017, 615-632.

[27] Barati, M.R., Shahverdi, H., Aero-hygro-thermal stability analysis of higher-order refined supersonic FGM panels with even and uneven porosity distributions, *Journal of Fluids and Structures*, 73, 2017, 125–136.

[28] Chen, D., Yang, J., Kitipornchai, S., Nonlinear vibration and postbuckling of functionally graded graphene reinforced porous nanocomposite beams, *Composites Science and Technology*, 142, 2017, 235-245.

[29] Ebrahimi, F., Jafari, A., Barati, M.R., Vibration analysis of magneto-electro-elastic heterogeneous porous material plates resting on elastic foundations, *Thin-Walled Structures*, 119, 2017, 33–46.

[30] Şimşek, M., Aydın, M., Size-Dependent Forced Vibration of an Imperfect Functionally Graded (FG) Microplate with porosities Subjected to a moving load using the modified couple stress theory, *Composite Structures*, 160, 2016, 408-421.

[31] Shahverdi, H., Barati M.R., Vibration analysis of porous functionally graded nanoplates, *International Journal of Engineering Science*, 120, 2017, 82–99.

[32] Akbaş, S.D., Vibration and static analysis of functionally graded porous plates, *Journal of Applied and Computational Mechanics*, 3(3), 2017, 199-207.

[33] Shojaeefard, M.H., Googarchin, H. S., Ghadiri, M., Mahinzare, M., Micro temperature-dependent FG porous plate: Free vibration and thermal buckling analysis using modified couple stress theory with CPT and FSDT, *Applied Mathematical Modelling*, 50, 2017, 366-355.

[34] Wang, Y.Q., Wan, Y.H., Zhang, Y.F., Vibrations of longitudinally traveling functionally graded material plates with porosities, *European Journal of Mechanics / A Solids*, 66, 2017, 55-68.

[35] Wang, Y., Wu, D., Free vibration of functionally graded porous cylindrical shell using a sinusoidal shear deformation theory, *Aerospace Science and Technology*, 66, 2017, 83-91.

[36] Ziane, N., Meftah, S.A., Ruta, G., Tounsi, A., Thermal effects on the instabilities of porous FGM box beams, *Engineering Structures*, 134, 2017, 150–158.

[37] Duc, N.D., *Nonlinear Static and Dynamic Stability of Functionally Graded Plates and Shells*, Vietnam National University Press, Hanoi, Vietnam, 2014.

[38] Reddy, J.N., *Mechanics of laminated composite plates and shells: theory and analysi*s, Boca Raton, CRC Press, 2004.

Appendix I

$$H_{11}(w) = \frac{\kappa E_1}{2(1+\nu)}\frac{\partial^2 w}{\partial x^2} + \frac{\kappa E_1}{2(1+\nu)}\frac{\partial^2 w}{\partial y^2} - K_w w + K_p\left(\frac{\partial^2 w}{\partial x^2} + \frac{\partial^2 w}{\partial y^2}\right),$$

$$H_{12}(\phi_x) = \frac{\kappa E_1}{2(1+\nu)}\frac{\partial \phi_x}{\partial x}, H_{13}(\phi_y) = \frac{\kappa E_1}{2(1+\nu)}\frac{\partial \phi_y}{\partial y},$$

$$P(w,f) = \frac{\partial^2 f}{\partial y^2}\frac{\partial^2 w}{\partial x^2} - 2\frac{\partial^2 f}{\partial x \partial y}\frac{\partial^2 w}{\partial x \partial y} + \frac{\partial^2 f}{\partial x^2}\frac{\partial^2 w}{\partial y^2}, \rho_0 = I_0, \rho_1 = I_2 - \frac{I_1^2}{I_o},$$

$$H_{21}(w) = -\frac{\kappa E_1}{2(1+\nu)}\frac{\partial w}{\partial x},$$

$$H_{22}(\phi_x) = \frac{1}{1-\nu^2}\left(E_3 - \frac{E_2^2}{E_1}\right)\frac{\partial^2 \phi_x}{\partial x^2} + \frac{1}{2(1+\nu)}\left(E_3 - \frac{E_2^2}{E_1}\right)\frac{\partial^2 \phi_x}{\partial y^2} - \frac{\kappa E_1}{2(1+\nu)}\phi_x,$$

$$H_{23}(\phi_y) = \frac{1}{2(1-\nu)}\left(E_3 - \frac{E_2^2}{E_1}\right)\frac{\partial^2 \phi_y}{\partial x \partial y},$$

$$H_{31}(w) = -\frac{\kappa E_1}{2(1+v)}\frac{\partial w}{\partial y}, H_{32}(\phi_x) = \frac{1}{2(1-v)}\left(E_3 - \frac{E_2^2}{E_1}\right)\frac{\partial^2 \phi_x}{\partial x\,\partial y},$$

$$H_{33}(\phi_y) = \frac{1}{2(1+v)}\left(E_3 - \frac{E_2^2}{E_1}\right)\frac{\partial^2 \phi_y}{\partial x^2} + \frac{1}{1-v^2}\left(E_3 - \frac{E_2^2}{E_1}\right)\frac{\partial^2 \phi_y}{\partial y^2} - \frac{\kappa E_1}{2(1+v)}\phi_y.$$

Appendix II

$$h_{11} = -\left[\frac{\kappa E_1}{2(1+v)}\left(\frac{m\pi}{a}\right)^2 + \frac{\kappa E_1}{2(1+v)}\left(\frac{n\pi}{b}\right)^2 + K_w + K_p\left(\left(\frac{m\pi}{a}\right)^2 + \left(\frac{n\pi}{b}\right)^2\right)\right],$$

$$h_{12} = -\frac{\kappa E_1}{2(1+v)}\frac{m\pi}{a}; \quad h_{13} = -\frac{\kappa E_1}{2(1+v)}\frac{n\pi}{b},$$

$$h_{21} = -\frac{\kappa E_1}{2(1+v)}\frac{m\pi}{a}, h_{22} = -\left(E_3 - \frac{E_2^2}{E_1}\right)\left[\frac{1}{1-v^2}\left(\frac{m\pi}{a}\right)^2 + \frac{1}{2(1+v)}\left(\frac{n\pi}{b}\right)^2\right] - \frac{\kappa E_1}{2(1+v)},$$

$$h_{23} = -\frac{1}{2(1-v)}\left(E_3 - \frac{E_2^2}{E_1}\right)\frac{mn\pi^2}{ab},$$

$$h_{31} = -\frac{\kappa E_1}{2(1+v)}\frac{n\pi}{b}, h_{32} = -\frac{1}{2(1-v)}\left(E_3 - \frac{E_2^2}{E_1}\right)\frac{mn\pi^2}{ab},$$

$$h_{33} = -\left(E_3 - \frac{E_2^2}{E_1}\right)\left[\frac{1}{2(1+v)}\left(\frac{m\pi}{a}\right)^2 + \frac{1}{1-v^2}\left(\frac{n\pi}{b}\right)^2\right] - \frac{\kappa E_1}{2(1+v)}$$

$$n_1 = -\frac{E_1}{16}\left(\left(\frac{m\pi}{a}\right)^4 + \left(\frac{n\pi}{b}\right)^4\right), n_2 = -\left(\frac{m\pi}{a}\right)^2, n_3 = \frac{16}{mn\pi^2}, n_4 = -\left(\frac{n\pi}{b}\right)^2.$$

$$h_{14} = -(n_2 + vn_4)\frac{4E_2}{an\pi(1-v^2)}; \quad h_{15} = -(n_2 v + n_4)\frac{4E_2}{bm\pi(1-v^2)},$$

$$h_{16} = \left(\frac{n\pi}{b}\right)^2\frac{(vn_2 + n_4)E_1}{8(1-v^2)} + \left(\frac{m\pi}{a}\right)^2\frac{(n_2 + vn_4)E_1}{8(1-v^2)} + n_1.$$